INTERIM REPORT ON DIVERTOR AND GAS BLANKET IMPURITY CONTROL STUDY*

by

Z. El Derini and W. M. Stacey, Jr.
School of Nuclear Engineering
Georgia Institute of Technology
Atlanta, Georgia 30332

* Work supported by U.S. Department of Energy under Contract No. ET-78-S-05-5683 with Georgia Institute of Technology.

DIVERTOR AND GAS BLANKET PERFORMANCE STUDY

Abstract

A simple calculational model for the transport of particles across the "scrape off" region between the plasma and the wall in the presence of a divertor or a gas blanket has been developed. The model departs from previous work in including: a) the entire impurity transport as well as its effect on the energy balance equations; b) the recycling neutrals from the divertor, and c) the reflected neutrals from the wall. Results obtained with this model show how the steady state impurity level in the plasma depends on the divertor parameters such as the neutral backflow from the divertor, the particle residence time and the "scrape off" thickness; and on the gas blanket parameters such as the neutral source strength and the gas blanket thickness. The variation of the divertor or gas blanket performance as a function of the heat and particle fluxes escaping from the plasma, the wall material and the cross field diffusion is examined and numerical examples are given. This work contributes to an understanding of the divertor and gas blanket parameters that are required in order to efficiently shield the plasma and it also helps to indicate new methods for improving the effectiveness of divertors and gas blankets.

Introduction

Active impurity control may be necessary in tokamak reactors (e.g. Refs. 1-4) since the presence of impurities will affect the operation of fusion reactors as follows: a) impurities enhance radiation losses; b) reduce the ion density, and this will, in turn, result in a decrease of thermonuclear reaction rate and an increase in ignition temperature; c) shift the Lawson and ignition criteria towards higher temperature; d) increase the requirement on neutral beam energy for penetration; and f) possibly cause some instability due to edge cooling.

Various methods have been proposed to control the impurity concentration in the plasma. Among these are divertors[5-9] and neutral gas blankets.[10-15]

Theoretical studies on both divertors and gas blankets have previously been performed by several authors. These studies followed different approaches. For example, in the case of the divertor: 1) a neoclassical treatment with the assumption of hot ions and cold electrons was given by Hinton,[16] et al.; 2) two fluid Braginskii equations with warm electrons and cold ions were used by Boozer,[17] 3) others developed a model[18-20] where the diffusion parallel to the magnetic field was approximated in the particle continuity equation by an absorption term equal to $\frac{\Gamma_{||}}{L(r)}$, where L(r) is an average distance traveled along a field line to the collector plate, and $\Gamma_{||}$ is the particle flux along the magnetic field line. The particle flux, $\Gamma_{||}$, was assumed to be ambipolar and an electrostatic field would be established which would enhance the electron parallel heat flux, $Q_{||}^{e}$. In this model,[18-20] the charge exchange neutrals were included,

but both impurities and recycled neutrals from the wall were neglected. Most of the studies on gas blanket,[10-15] did not take impurity into consideration and neglected radiation losses as well as recombination.

In this paper, a semi-analytical model to describe both divertor and gas blanket is formulated and written into a computer program capable of predicting the performance of a divertor or a gas blanket. The model involves the solution of the space dependent (ion and impurity) continuity equations and the energy conservation equations self-consistently with the neutral transport equation. The model includes an entire impurity transport calculation as well as its effect on the energy balance equations. The recycled neutrals from the divertor, as well as those reflected from the first wall, are treated. In Section II, the model used to describe the particle and energy transport in the "scrape off" region between the plasma and the wall is discussed. A study of the sensitivity of divertor and gas blanket performance to the particle and heat fluxes escaping from the plasma, the reflection coefficient, the external neutral source, the cross-field diffusion coefficient and the residence time is presented in Section III. This study outlines the different phenomena that determine the effectiveness of a divertor or a gas blanket and provides the range of divertor or gas blanket parameters that are required to achieve a given level of impurity control. Conclusions drawn from this study are summarized in Section IV.

II. Model description

We represent the divertor "scrape off" region or the gas blanket by a slab model extending from the plasma interface (separatrix for a

divertor) located at $x = 0$ to the first wall located at $x = \delta_s$. The particle, Γ_p, and heat, Q_p, fluxes escaping from the plasma define the boundary conditions at $x = 0$, and the reflection and sputtering properties of the wall are used to define the boundary at $x = \delta_s$. Another boundary condition is obtained by specifying either the ion density or the ion flux at the wall to be zero. The plasma ion density at the plasma boundary is determined by the calculations. We treat the cross field transport of neutral and ionized particles of the main plasma and of the wall sputtered impurity species, the cross field transport of heat, the loss of energy due to radiative and other atomic processes, and the transport of particles and energy along field lines into the divertor chamber in our model of the scrape off region/gas blanket.

In order to model the parallel loss in the "scrape-off" region, we postulate that the residence time, $\tau_{||}$, for an ion is given by $\tau_{||} = \frac{\tau^0_{||}}{\sqrt{T}}$ with $\tau^0_{||}$ given. This choice is motivated by the physical model $\tau_{||} \simeq \frac{L_{||}}{v_s}$, where $L_{||}$ is the mean distance traveled along the magnetic field line to the collector plate and v_s is the ion flow velocity. This situation holds for divertors where the divertor chamber and the field null are located on the outside of the torus. Since the electron velocity is much larger than the ion velocity, an electrostatic sheath will be formed at the collector which impedes the parallel diffusion of the electrons so that the net electrical current vanishes at the collector. This potential is included to obtain an electron energy loss enhancement factor:

$$\gamma_e = 1 + \frac{1}{2} \ln \left(\frac{1}{\frac{n_i}{n_e}\left(\frac{T_i m_e}{T_e m_i}\right)^{\frac{1}{2}} + \frac{z n_z}{n_e}\left(\frac{T_z m_e}{m_z T_e}\right)^{\frac{1}{2}}} \right)$$

where n, T, m, and z are the density, temperature, mass, and charge, and the subscripts i, e, z stand for ion, electron, and impurity, respectively. Including this enhancement factor, the electron heat flux to the divertor can be written as

$$Q_{||e} = 2kT_e \gamma_e \Gamma_{||e}$$

where $\Gamma_{||e}$ is the electron flux along the field line.

The cross field diffusion is taken to be Bohm diffusion with a variable coefficient. This choice implies the presence of low frequency turbulence in the boundary region which can arise due to steep gradients.

The ion density satisfies

$$\frac{d}{dx}\left(-D_{\perp}\frac{dn_i}{dx}\right) + \frac{n_i}{\tau_{||i}} - n_e n_{|c_h|} \langle\sigma v\rangle_i |_{c_h|} + n_e n_i \langle\sigma v\rangle_R = 0 \qquad (1)$$

where $D_{\perp} = \frac{F\, kT_e}{16_e B}$, F is a variable coefficient, $\tau_{||i}$ is the ion residence time (the second term in the equation is zero in the case of a static neutral gas blanket), n_e, n_i, n_c, and n_h are the electron, ion, cold and hot neutral densities respectively, $\langle\sigma v\rangle_i$ and $\langle\sigma v\rangle_R$ are the electron impact ionization rate and recombination rate.

One of the major categories where input information is required for the plasma model described above is atomic physics characterizing the ionization and charge exchange cross section. Atomic cross section,[21-24] are available for charge exchange for D-T neutrals with D-T ions and collisional ionization for D-T neutrals by electrons and D-T ions. The ionization and charge exchange rates used in this work are taken from reference 25.

Neglecting recombination compared to the losses along the field line in the case of a divertor, the ion continuity equation can be written as:

$$\frac{d^2 n_i}{dx^2} + k^2(x)\, n_i\,(x) = 0, \tag{2}$$

where $k^2(x)$ may be negative at $x = 0$ then increases to zero at $x = b$ where b is defined by $k^2(b) = 0$, and it is the location where the ionization term is equal to the loss along the field line. Equation (2) has the approximate solution

$$n_{i1}(x) = A \exp\left(-\int_o^x k dx'\right) + B \exp\left(\int_o^x k dx'\right) \qquad o \leq x \leq b \tag{3}$$

$$n_{i2}(x) = C \cos\left(\int_b^x k dx'\right) + D \sin\left(\int_b^x k dx'\right) \qquad b \leq x \leq \delta_s \tag{4}$$

where A, B, C, and D are determined by using the following boundary conditions:

a) continuous particle flux at the plasma boundary,

b) continuous particle flux at $x = b$,

c) continuous particle density at $x = b$,

d) and $\Gamma_i(\delta_s)$ or $n_i(\delta_s) = 0$ at the wall.

In case where $k^2(x)$ is a slowly varying function of x, Eq. (2) has been solved using the WKB[26-28] approximation. This yields the following analytical solution:

$$n_{i1}(x) = \frac{c_1}{\sqrt{k}}\left(2 \sin\phi\, e^{\int_x^b k dx} + \cos\phi\, e^{-\int_x^b k dx}\right) \qquad o \leq x \leq b \tag{5}$$

$$n_{i2}(x) \approx \frac{2c_1}{\sqrt{k}}\left[\cos\left(\int_b^x k dx - \frac{\pi}{4} + \phi\right)\right] \qquad b \leq x \leq \delta_s \tag{6}$$

where $c_1 = \dfrac{\Gamma_i(x=0)}{D_\perp \sqrt{k(o)} \left(2 \sin \phi \; e^{\int_o^b k dx} - \cos \phi \; e^{-\int_o^b k dx} \right)}$ (7)

and ϕ is determined from the boundary condition at the first wall, we also have two options, either $\Gamma_i(\delta_s) = 0$ or $n_i(\delta_s) = 0$. The results in the scrape off region have been found not to be generally sensitive to the boundary condition at the wall.

For a neutral gas blanket, the recombination term cannot be neglected, and the ion continuity equation can be written as

$$\frac{d^2 n_i}{dx^2} = \frac{n_i^2}{\gamma^2} - \frac{n_i}{\lambda^2} \tag{8}$$

where $\gamma^2 = \dfrac{D_i}{R_1 \langle \sigma v \rangle_R}$, $\lambda^2 = \dfrac{D_i}{n_h \langle \sigma v \rangle_{ih} R_1 + n_c \langle \sigma v \rangle_{ic} R_1}$

and $R_i = \dfrac{n_e}{n_i}$.

The solution is expressed as

$$\int_{n_o}^{n} \frac{dn_i}{\sqrt{n_i^2 (n_i - \xi) + c_o}} = -\sqrt{\frac{2}{3}} \int_o^x \frac{dx}{\gamma} \tag{9}$$

where $\xi = \dfrac{3}{2} \left(\dfrac{\gamma}{\lambda}\right)^2$

The solution is an elliptic function where the constants c_o and n_o are determined from the following boundary conditions: a) total plasma flux across the separatrix has to equal the total loss of confined plasma, and b) zero ion density at the first wall.

Ions and electrons diffusing from the plasma interact with the limiter. This can give rise to desorption and backstreaming of neutrals as well as evaporation and sputtering at the limiter. Likewise, charge exchange neutrals interact with the vacuum chamber liner or first wall and cause reflection of hydrogenic neutrals. These cold neutral atoms are assumed to come off the wall isotropically. As they proceed across the boundary, many get ionized by electrons and ions, or charge exchange with ions to form neutral atoms with energies corresponding to the plasma energy. Therefore, the cold neutrals experience ionization and charge exchange, which are equivalent to capture and scattering with cold neutral, respectively, in neutron transport theory. Therefore, the problem of penetration and interaction of neutrals with plasma is solved here using a one group neutron transport equation[29] given by

$$\mu \frac{\partial F}{\partial x} + \Sigma_t F = \frac{1}{2} \Sigma_s \phi + \frac{1}{2} s, \tag{10}$$

where F is the neutral angular flux, μ is the cosine of the angle between the neutral velocity and the x axis, Σ_t and Σ_s are the total and scattering cross section, ϕ is the neutral flux given by

$$\phi(x) = \int_{-1}^{1} F(x,\mu) d\mu ,$$

and s is the neutral source.

Equation (10) is solved by the discrete ordinates method subject to the following boundary conditions:

a) $F_{i,\, n+1} = 0 \qquad$ for $\mu_i < o$

b) $F_{i,\, 1} = 0 \qquad$ for $\mu_i > o$

where n + 1 and 1 refer to the wall and the separatrix, respectively. These boundary conditions imply that no returning neutral flux from the wall and no cold neutrals come from the plasma to the boundary region at x = 0. Boundary condition (b) is always true since at the separatrix the neutral density is small and the absorption cross section is much higher than the scattering cross section. The cold neutral source, s, is assumed to be isotropic and of magnitude proportional to

$$R_d \int_o^{\delta_s} \frac{n_i dx}{\tau_{ii}} + R_w \left(\Gamma_{cxw} + \Gamma_w\right) + \Gamma_{ex},$$

where R_d is the backflow fraction from the divertor, R_w is the wall reflection coefficient, Γ_{cx} is the flux of charge exchange neutrals incident upon the wall.

$$\Gamma_{cx} = \alpha_{cx} \int_o^{\delta_s} n_i n_o \langle \sigma v \rangle_{cx} \, dx, \tag{11}$$

Γ_w is the plasma flux incident on the wall, and Γ_{ex} is due to gas puffing. In Eq. (11), $\langle \sigma v \rangle_{cx}$ is the charge exchange rate and α_{cx} is the probability that a charge exchange neutral strikes the wall. A two generations estimate of α_{cx} is

$$\alpha_{cx} = \frac{1}{2}\left(1 + \frac{1}{2}\,\frac{1}{\left(1 + \frac{\langle \sigma v \rangle_i}{\langle \sigma v \rangle_{cx}}\right)}\right) \tag{12}$$

The hot neutral profile has also been calculated, in the case of a neutral gas blanket, by solving the one group transport equation by discrete ordinates subject to the following boundary conditions:

a) $F_{i,n+1} = 0$ for $\mu_i < o$, i.e. no return from the wall,

b) $F_{NP,1} = KF_{NP+1-i,1}$ for $\mu_i < o$, i.e. reflective boundary at $x = 0$

with albedo equal K,

where NP is half the number of discrete angle and K is a constant less than or equal to unity.

Sputtering of the first wall due to charge exchange neutrals was calculated using sputtering yield, γ^w, as a function of the ion energy.[25] This sputtering yield has been obtained by averaging the monoenergetic sputter yields over a Maxwellian distribution of incident particle energies and then interpolated as a function of ion energy. Impurity atoms are assumed to come off the wall isotropically. Since no data are available on the energy spectrum of the sputtered impurity atoms, this energy is taken to be equal to 1 eV. The inwards neutral impurity atoms, $\gamma^w \Gamma_{cx}$, is attenuated by ionization according to

$$n_{nz} v_{nz} = \gamma^w \Gamma_{cx} E_1 \left(\int_x^{\delta s} (z n_z + n_i) \frac{\langle \sigma v \rangle_{ze}}{v_{nz}} dx' \right) \tag{13}$$

where $\langle \sigma v \rangle_{ze}$ is the impurity ionization rate and the subscript nz and z refer to impurity atoms and ions, respectively. The impurity ions satisfy

$$\frac{d}{dx} \left(- D_{\perp z} \frac{dn_z}{dx} \right) + \frac{n_z}{\tau_{\parallel z}} = n_e n_{nz} \langle \sigma v \rangle_{ze} = S_z \tag{14}$$

The solution to Eq. (14) is constructed using the Green's function for a unit source at $x = x_o$. This Green's function satisfies:

$$- D_{\perp z} \frac{d^2\phi_z(x,x_o)}{dx^2} + \frac{\phi_z(x,x_o)}{\tau_{\|z}} = 0.$$

The appropriate boundary conditions follow from the fact that the impurity ion density vanishes at the wall because of electronic recombination at the surface, and from assuming a reflecting boundary condition at the plasma boundary, which is based on the assumption of zero net impurity flux across the interface in equilibrium. Thus, $n_z(\delta_s) = 0$ and $\frac{dn_z(o)}{dx} = 0$ lead to $\phi_z(\delta_s,x_o)$ and $\frac{d\phi_z}{dx}(o,x_o) = 0$. Since $\phi_z(x,x_o)$ is the Green's function for a unit source located at $x = x_o$, it must also satisfy the source condition

$$\lim_{\varepsilon\to 0} D_{\perp z} \int_{x_o-\varepsilon}^{x_o+\varepsilon} \left(\frac{d}{dx}\phi_z(x,x_o)\right) dx = 1.$$

The Green's functions which satisfy these boundary conditions are given by:

$$\phi^-(x,x_o) = \frac{\cosh K_z(\delta_s - x_o)\ \cosh K_z x}{D_{\perp z} K_z \cosh(K_z\delta_s)}$$

$$\phi^+(x,x_o) = \frac{\cosh K_z(\delta_s - x_o)\ \cosh K_z x_o\ \sinh K_z(\delta_s - x)}{D_{\perp z} K_z \cosh(K_z\delta_s)\ \sinh K_z(\delta_s - x_o)}.$$

The impurity ion profile can be written as

$$n_z(x) = \int_o^x \frac{\cosh K_z(\delta_s - x_o) \cosh (K_z x_o) \sinh K_z(\delta_s - x) S_z(x_o)\, dx_o}{D_{\perp z} K_z \cosh (K_z \delta_s) \sinh K_z(\delta_s - x_o)}$$

$$+ \int_x^{\delta_s} \frac{\cosh K_z(\delta_s - x_o) \cosh (K_z x) S_z(x_o)\, dx_o}{D_{\perp z} K_z \cosh (K_z \delta_s)}, \qquad (16)$$

where $K_z = (D_{\perp z}\, \tau_{\parallel z})^{-\frac{1}{2}}$.

The previous equation is valid only in the presence of a divertor. For a static gas blanket the impurity ion profile is

$$n_z(x) = \int_o^{\delta_s} \left[\int_o^{x'} \frac{S_z dy}{D_{\perp z}} \right] dx' - \int_o^{x} \left[\int_o^{x'} \frac{S_z dy}{D_{\perp z}} \right] dx'. \qquad (17)$$

This equation is obtained by solving Eq. (14) with $\frac{n_z}{\tau_{\parallel z}}$ equal to zero and subject to the following conditions of a) $n_z(\delta_s) = 0$, and b) $\frac{dn_z}{dx}\Big|_{x=o} = 0$.

The heat flow equations for ions and electrons are:

$$-\frac{dQ_e}{dx} + \frac{\gamma_e n_e T_e}{\tau_{\parallel}} + W_{rad} + EL - c_1 n_i n_e \left(\frac{T_i - T_e}{T_e^{3/2}} \right) = 0, \qquad (18)$$

$$-\frac{dQ_i}{dx} + \frac{n_i T_i}{\tau_{\parallel}} + 2\, n_i n_o \langle \sigma v \rangle_{cx}\, \alpha_{cx}(1 - \alpha_e)\, T_i + c_1 n_i n_e \left(\frac{T_i - T_e}{T_e^{3/2}} \right) = 0, \qquad (19)$$

where Q is the heat flux, W_{rad} is the radiated power by bremstrahlung, line and recombination processes, α_e is the energy reflection coefficient of the wall, and EL is the total energy loss due to ionization and exitation. In the model the radiative power loss, P_z, is computed as

$$P_z = n_e n_z L_z,$$

where L_z is computed from the polynomial fit of D. E. Post et al.[31] Bremstrahlung[32] radiation is also included and equals to

$$P_{Brem} = 1.5 \times 10^{-32} Z_{eff} n^2 \left(T_e(ev)\right)^{\frac{1}{2}} \quad w/cm^3.$$

Therefore, the total radiated power, $W_{rad} = P_{Brem} + P_z$. In the case of a neutral gas blanket, an additional term, which represents the heat loss by elastic collision with neutrals, is incorporated into the heat equation. This term is equal to $(T_i - T_n)\, m_i \nu_{in} f_{in}$, where ν_{in} is the collision frequency of ions with neutrals , f_{in} represents the fraction of heat being lost by elastic collision, T_i and T_n are the ion and neutral temperature, respectively. Equations (18) and (19) are integrated over the boundary region, assuming average temperature T_e and T_i for the entire zone and that $Q(\delta_s)$ vanishes at the wall, and then solved for the average temperatures in the boundary region.

III. Analysis

The model described in the previous section was used to study the performance of the "scrape off" region as a function of the plasma, "scrape off" region and wall parameters. The principal plasma parameters considered are the heat and particle fluxes out of the plasma. For the

"scrape off" region, the magnetic field, the physical thickness, the residence time and the backflow from the divertor are the main parameters. The wall material, the reflection coefficient from the wall and the external neutral source are the major wall parameters. For the purpose of this analysis, the main scrape off/gas blanket and wall parameters are taken to be: toroidal magnetic field, 30 KG; reflected neutral temperature, 1 eV; impurity temperature, 4 eV; and carbon liner or stainless steel first wall. In Fig. 1 we plotted the ion, cold neutral and impurity profiles for a typical divertor case as a function of the depth in the "scrape off" region, x. Figure 2 shows the ion, cold and hot neutral, and impurity profile for a neutral gas blanket as a function of x. In order to display examples of the performance of a divertor, we chose the following parameters:

1. $\frac{Q_w}{Q_p}$ is the fraction of the heat energy flowing from the plasma into the "scrape off" region that subsequently reaches the first wall either as radiative energy or by charge exchange neutrals.

2. $\left(\frac{\Gamma_{cxw} + \Gamma_{iw}}{\Gamma_p}\right)$ is the ratio of the sum of the particle fluxes which hits the wall as charge exchange neutral, Γ_{cxw}, and ions, Γ_{iw}, to the ion flux, Γ_p, escaping from the plasma.

3. $n_z(o)$ is the impurity concentration at the plasma boundary, $x = o$. Thus, $\frac{n_z(o)}{\Gamma_p}$ provides a relative measure of the impurity concentration in the plasma, normalized to the magnitude of the particle flux out of the plasma.

4. The unload efficiency, η^u, for the divertor - a small η^u implies that a large fraction of the plasma flux will hit the wall.

5. The ionization probability, P^i_{DT} or P^i_z, defined as the probability that a neutral coming from the wall will be ionized before reaching the separatrix; subscript DT and z refer to deuterium-tritium and impurity, respectively.

6. P_d is the probability that an impurity ion in the "scrape off" region is swept into the divertor and is defined as

$$P^d = \frac{\Gamma_z^{div}}{\int_o^{\delta_s} S_I dx}$$

where Γ_z^{div} is the impurity flux to the divertor and S_I is the impurity source strength in the "scrape off" region.

For a neutral gas blanket, the parameters $\frac{Q_w}{Q_p}$, $\left(\frac{\Gamma_{cxw} + \Gamma_{iw}}{\Gamma_p}\right)$, and $\frac{n_z(o)}{\Gamma_p}$ are used. The results for the divertor and gas blanket are discussed next using the parameters just defined.

A. Divertor

1. Heat flow out of the plasma

Tables 1 and 2 show the variation in the divertor performance parameters with the heat flux, Q_p, out of the plasma. The results in Table 1 are for graphite liner, while those in Table 2 are for stainless steel first wall. The explanation of the results in Tables 1 and 2 follows:

a. The fraction of heat energy flowing from the plasma, $\frac{Q_w}{Q_p}$, into the "scrape off" region that subsequently reaches the first wall is small, therefore the major heat loss in the boundary region is by transport to the divertor.

b. The radiated power, Q_{rad}, is small for carbon and large for iron. As the heat flow out of the plasma, Q_p, is reduced, the average temperature of the "scrape off" region decreases and the radiation losses increase since W_{rad} peaks at low electron temperature. This explains why $\left(\frac{Q_w}{Q_p}\right)$ decreases for iron as Q_p increases.

c. For the same particle flux, Γ_p, out of the plasma as Q_p increases, the average temperature increases as does the cross field diffusion coefficient and this will lower the ion density in the "scrape off" region.

d. As Q_p is increased, the particle flux that hits the first wall reaches a maximum and then decreases. This behavior is due to the fact that both the particle flux to the divertor, Γ_{idiv}, and the ionization rate increase and then decrease due to the variation in the particle density and the average temperature of the "scrape off" region.

e. The impurity concentration, $n_z(o)$, at the separatrix decreases as Q_p increases. This is mainly due to the fact that the ion particle density decreases, which in turn will decrease the ionization probability and consequently the impurity source.

f. The unload efficiency, η^u, has a minimum for both carbon and iron wall. It follows the opposite trend of the particle flux to the wall.

g. These two sets of parameters in Tables 1 and 2 represent a good example for high ionization probability, P_z^i. Note that P^i decreases as Q_p increases because of the decrease in the ion particle density.

h. Steady state solution exists only for $Q_p \geq 3.0 \times 10^4$ w/m^2 for carbon and greater than 1.0×10^5 w/m^2 for iron. Physically this lower boundary comes from the fact that the heat flux out of the plasma is insufficient to sustain the losses due to radiation, charge exchange and transport to the divertor zone.

k. For a given heat flux out of the plasma, the electron temperature drops faster than the ion temperature in the "scrape off" region. The difference $(T_i - T_e)$ in the divertor zone is caused by a) the sheath potential at the collector which leads to preferential collection of high energy electrons, b) radiation losses and c) is due to the fact that the ion-electron equilibration is small due to the low particle density in the "scrape off" region. For most of the following examples, Q_p is taken to be .16 Mw/m^2 and these results are more appropriate for present and next generation tokamaks.

2. Particle flux out of the plasma

The effect of the particle flux out of the plasma, Γ_p, on the divertor performance is summarized in Tables 3 and 4. As the particle flux decreases the particle density in the "scrape off" region decreases and these conclusions follow:

a. the heat and particle fluxes to the wall decrease; the initial increase of $\frac{Q_w}{Q_p}$ for carbon is due to the fact that for the same Q_p, the heat loss to divertor decreases;

b. the impurity concentration in the plasma decreases, as does the ionization probability;

c. the unload efficiency, η^u, increases;

d. the average temperature in the "scrape off" region increases, i.e. temperature drops slowly.

3. Cross field diffusion

Reducing $D_\perp$ causes the ion density to drop faster in the boundary region for a given particle flux, Γ_p, from the plasma. It also produces higher separatrix densities. Tables 5.A and 5.B show the divertor parameters for different values of $D_\perp$. We notice, from Table 5.B, that the impurity level in the plasma and the unload efficiency increase as $D_\perp$ is reduced and that the ionization probability does not change significantly with $D_\perp$. Therefore, for low neutral backflow, R_d, and reflection, R_w, coefficients, the cross field diffusion should be enhanced in order to shield the plasma core efficiently. This procedure was suggested by W. Engelhardt.[33] However, if R_w is unity, the impurity level is almost constant, independent of the cross field diffusion coefficient, as indicated in Table 5.A. From Table 6 we notice that by keeping $\frac{\delta}{\sqrt{D}}$ constant, the parameters $\frac{Q_w}{Q_p}$, $\frac{\Gamma_{iw} + \Gamma_{cxw}}{\Gamma_p}$, η^u, P^i_{dt}, and P^z_{dt} remains unchanged, but low impurity concentration corresponds to high values of both δ_s and D.

4. Residence time, $\tau_{||}$

Table 7 summarizes the divertor parameters obtained for carbon for different residence time, $\tau_{||}$. A few remarks on this table are: as $\tau_{||}$ increases, less particles will go to the divertor and the particle density in the "scrape off" region increases, this will lead to an increase in the particle and heat fluxes to the wall, in the impurity density, and in the ionization probability, and also will decrease the unload efficiency. From this table we can conclude that for a given flux the higher the residence time, the better the ionization probability. Therefore, one possibility for improving the ionization probability in

the "scrape off" region is to increase the geometric path length, L, into the divertor. However, we notice also that by increasing L, the impurities will penetrate the "scrape-off" region more readily.

$\tau_{||}$ is chosen to be one order of magnitude higher for carbon than for iron. This choice is due to the fact that the "scrape off" thickness is taken to be the same for both carbon and iron. In other words, the ion residence time in the divertor should be lower for iron than carbon for the same scrape off thickness. Table 8 shows that the divertor parameters are not very sensitive to δ_s or $\tau_{||}$ if the ratio $\frac{\delta_s}{\tau_{||}}$ is kept constant.

5. Scrape off thickness

Tables 9 and 10 show the variation of the boundary region characteristics as a function of the "scrape off" thickness. Table 9 is for carbon and 10 for iron. Some remarks on these tables are as follows:

1. The heat flux to the wall reaches a maximum and then decreases as δ_s increases. This can be explained by the fact that the average temperature of the boundary region decreases as δ_s increases, while the charge exchange flux and the particle density increases.
2. The particle flux to the wall has the same behavior as the heat flux to the wall, because the particle flux and the ionization rate increases as δ_s increases.
3. The unload efficiency follows an inverse behavior of Γ_{iw}.
4. As δ_s increases, the ion density increases, as does the ionization probability.

The "scrape off" thickness is one of the most important parameters which controls the performance of the divertor. As mentioned previously, in order to shield the plasma efficiently we have to increase δ_s as $D_\perp$ increases.

6. Neutral return from the divertor

A fraction, R_d, of the plasma ions that are collected by the divertor is recycled back to the plasma as cold H_2 molecules. The effect of the reflection coefficient, R_d, on the divertor performance is shown in Table 11.

As the reflection coefficient decreases, the particle density in the scrape off region decreases. This will decrease both the heat and particle fluxes to the wall and the impurity concentration in the plasma and increase the unload efficiency. The ionization probability is almost unaffected. Therefore, efficient divertor operation requires that only a small fraction of the neutrals generated in the divertor should return to the plasma.

7. External neutral source

In Fig. 3 the ion profile in the boundary has been drawn for two different values of external cold neutral source, S_{ex}, for carbon. The solid line shows the profile in the absence of an external neutral source, while the dotted one is for S_{ex} equal to 1E20 m^{-2} sec^{-1}. Higher S_{ex} provides a relatively wide plasma profile which would shield the plasma core relatively well from the neutral impurity. The increase in S_{ex} will broaden the ion profile. This is due to the fact that the ionization rate increases. Therefore, it is clear from Fig. 3 that the particle density increases as S_{ex} increases; this explains the behavior

of the particle and heat fluxes, the impurity density, and the ionization probability of Table 12. For iron, $\frac{n_z(o)}{\Gamma_p}$ has a minimum for a neutral source equal to 1×10^{17} m^{-2} sec^{-1}, this is due to the fact that the ion flux to the divertor has a maximum at $S_{ex} = 1 \times 10^{17}$ m^{-2} sec^{-1}. It turns out that a small amount of gas puffing in the edge region will decrease the iron impurity in the plasma.

9. Wall reflection coefficient

A fraction, R_w, of the particles that hit the first wall will return back to the plasma as cold neutrals. The effect of both R_w and R_d on the divertor parameters are shown in Tables 14 and 15 for carbon liner and stainless steel first wall, respectively. As R_w and R_d increase, the neutral flux coming into the "scrape off" region from the wall and the divertor increases. This will raise the charge exchange flux, the heat flux to the wall, the impurity concentration and the ionization probability.

It is clear from the previous discussion that the divertor is capable of strongly lessening the impurity concentration in the plasma since it reduces the particle flux hitting the reactor first wall. Furthermore, part of the incoming impurity atoms are ionized in the "scrape off" layer and swept into the divertor zone.

Another method to suppress the sputtering and shield the hot plasma core against the influx of impurity is to inject a cold neutral gas. Next we will summarize the similarities and differences in our model between divertors and gas blankets.

a. Recombination rates have been neglected in the presence of a divertor, but included for a gas blanket where the temperature

of the boundary region is low.

b. In the case of a divertor, the energetic particles bombarding the wall are primarily charge exchange neutral particles. The flux of hot neutrals is calculated from Eq.(11) for a divertor and by solving the hot neutral one group transport equation for a neutral gas blanket.

c. In the case of a gas blanket, the heat loss from the plasma to the cold neutrals, as well as the recombination losses, are included in the heat equation.

d. In the case of a divertor, a steady state solution can be found for particle and heat fluxes out of the plasma characteristic of a near term fusion reactor. However, in order to get a steady state solution for a gas blanket, the particle flux has to be increased by almost one order of magnitude and the heat flux has to be decreased. A solution can be obtained for reactor-type heat fluxes ($10^6 w/m^2$) provided that the thickness of the neutral gas blanket is more than 1 m or provided that one to two orders of magnitude higher particle flux out of the plasma is present. Therefore, one can conclude that the neutral gas blanket is a convenient impurity control mechanism for low heat and high particle fluxes out of the plasma but that a steady-state gas blanket is an unlikely impurity control mechanism for a reactor.

Since the general performance of the blanket would not change as Q_p increases, we choose the following parameters for the study of the performance of the gas blanket which will be presented in the next section: ion flux out of the plasma, $.846 \times 10^{21}$ $m^{-2} sec^{-1}$; impurity temperature,

4 eV; neutral temperature, 1 eV; and heat flux out of the plasma $\simeq 10^4$ w/m^2.

B. Neutral gas blanket

1. Heat flow out of the plasma, Q_p

Tables 16 and 17 show the neutral gas blanket parameters as a function of Q_p for first-wall surfaces of carbon and iron, respectively.

Charge exchange heat with cold neutrals is the dominant heat loss mechanism. From column 2 of Tables 16 and 17 we notice that a large fraction of heat will reach the first wall through radiative energy or by the charge exchange neutrals. Other losses due to ionization, excitation, and heating the cold neutrals are of the order of 20%. We notice also from column 3 that $\frac{\Gamma_{iw} + \Gamma_{cxw}}{\Gamma_p}$ is greater than 1, this is due to charge exchange recycling in the gas blanket. The average temperature for this set of parameters is 400 eV for carbon and 700 eV for iron.

Similar to the divertor core, no steady state solution exists for $Q_p < 1.9 \times 10^4$ w/m^2 for carbon and 5.2×10^4 w/m^2 for iron. This is due to the fact that the energy out of the plasma is insufficient to cover for the losses due to charge exchange, radiation, ionization, and heating the cold neutrals. A similar result has also been obtained by Lehnert.[11]

The impurity density decreases as Q_p increases for carbon and it is almost constant for iron, for this set of parameters. The sputtering coefficient decreases for carbon and is almost constant for iron in

this case, this explains the behavior of the impurity concentration in the plasma. The ionization probability is high and almost 1 for the neutral impurity and cold H_2 molecules. Unlike the case of a divertor, the electron temperature is comparable to the ion temperature for carbon, and T_e is less than T_i for Fe where radiation losses are high.

For a fixed external cold neutral source, S_{ex}, particle flux out of the plasma, Γ_p, and neutral gas blanket thickness, δ_s, there is a minimum heat flux, Q_p, below which no steady state solution exists. In Fig. 4 we plotted the minimum heat flux, Q_p, as a function of δ_s, for an external neutral source equal to 4×10^{20} #/m^2sec and a carbon liner. From this figure one can draw some qualitative conclusions rather easily:

a. For a given heat flux, Q_p, and external neutral density, S_{ex}, the gas blanket thickness, δ_s, should be chosen such that the design point lies in region I and as close to the curve as possible in order to have the lowest blanket temperature.

b. The higher Q_p, the wider must be the neutral gas blanket thickness, δ_s, for comparable blanket effectiveness.

2. Particle flux out of the plasma

Tables 18 and 19 show the effect of decreasing the particle flux out of the plasma, Γ_p, on the boundary region parameters for both wall materials. Some remarks on these tables follow. The heat flux to the wall increases as Γ_p increases for iron. This is due to the increase in the radiated power. For carbon, the heat flux is almost constant. As Γ_p increases, the particle density decreases and so does the impurity

concentration in the plasma. For a fixed Q_p, S_{ex}, and δ_s, the possible range of variation of Γ_p in order to get a steady state solution is small. In other words, $x < \Gamma_p < y$, the lower boundary comes from the fact that the particle density is low so that the ion electron equilibration term is insufficient to exchange the available large energy between electrons and ions; steady state solution probably exists with sufficiently high T_e, but this would not be a realistic cool gas blanket; the upper boundary comes from the fact that the heat flow out of the plasma can't sustain the losses. These bounds depend mainly on the heat flux out of the plasma. They are also sensitive to the gas blanket thickness and the cross field diffusion coefficient.

3. Cross field diffusion coefficient

As the cross field diffusion coefficient, $D_\perp$, decreases, the ion density in the blanket region increases by almost a constant factor. This increase is due mainly to the low temperature of the boundary region and high ionization rate, and due to the fact that the particle flux out of the plasma is constant. Therefore, in order to lower the particle density at the edge of the plasma, $D_\perp$ has to increase or δ_s decrease. The heat and particle fluxes to the wall follow the same behavior as the divertor case. As $D_\perp$ decreases, the impurity concentration increases as a result of high particle density, i.e. high ionization probability. These conclusions are deduced from Tables 20 and 21. For iron $\left(\frac{Q_w}{Q_p}\right)$ increases as $D_\perp$ decreases; this is mainly due to the increase in the radiation losses.

4. External neutral source

Tables 22 and 23 present the blanket parameters for different external neutral source, S_{ex}. For this case, the heat flux to the wall is almost constant, the impurity concentration increases as S_{ex} increases because of the increase in the particle density of the boundary region.

In Fig. 5 we plotted the average temperature of the boundary region as a function of S_{ex} for three different gas blanket thickness δ_s, for carbon. Figure 5 shows that the temperature is almost constant for low neutral source and then drops sharply as S_{ex} increases. The flat portion of the curve is due to the fact that S_{ex} is still negligible compared to the reflected neutral from the wall due to ion bombardment.

Figure 6 shows the neutral source that is required to achieve a given blanket temperature as a function of the gas blanket thickness, δ_s, for a constant heat and particle flux escaping from the plasma. The conclusions which can be drawn from Fig. 6 are :

a. the higher the neutral source at the wall, the lower will be the average temperature of the boundary region;

b. for a given T, the neutral source decreases as δ_s increases;

c. there is a maximum neutral source shown by curve (a) above which no steady state solution exists.

In Fig. 7 Q_p is plotted as a function of the maximum external neutral source, S_{ex} for a gas blanket which equals 30 cm thickness. The curve gives the maximum S_{ex} above which no steady state solution exists. The maximum neutral source given by curve a of Fig. 6 for a given Q_p and

δ_s is determined by the same physics as the minimum Q_p for a given S_{ex} and δ_s.

5. Reflection coefficient

The behavior of the blankets parameters as a function of the reflection coefficient is similar to the divertor and can be summarized by the following: As R_w decreases, the particle density in the boundary region decreases, this will decrease the heat and particle fluxes to the wall as well as the level of the impurity ions in the plasma.

6. Gas blanket thickness

Table 24 shows that the impurity concentration decreases as δ_s increases for a carbon wall. For an iron wall, $n_z(o)$ reaches a maximum at δ_s = 25 cm as shown in Table 25. This behavior is due to the variation of the recombination and ionization rate as a function of temperature.

Figure 5 indicates that for a given S_{ex} and Q_p, the wider the scrape off thickness, the lower will be the average temperature. Once the particle and heat fluxes are out of the plasma, and the external neutral source is specified, a curve similar to the one in Fig. 4 can be generated and the gas blanket thickness can be easily determined.

IV. Summary and Conclusions

We have modeled the divertor/gas blanket in terms of plasma, wall and divertor/gas blanket parameters. The principal plasma parameters considered in this paper are the heat and particle fluxes escaping from the plasma. The wall material and reflection coefficient are the major wall parameters. The neutral gas blanket is characterized by the physical thickness and its neutral concentration, while the divertor is characterized by the "scrape off" thickness, the backflow coefficient

from the divertor and the particle residence time along the field line. Within the divertor/gas blanket region, we solved a coupled set of transport equations for D-T ions, impurity ions, D-T neutral and impurity atoms self consistently with the ion and electron energy transport equations. We have carried out a study using this model to examine the effect of the particle and heat fluxes out of the plasma on the performance of the divertor/gas blanket. A combination of divertor backflow, wall reflection, and gas puffing at the wall are examined. Various residence times and cross field diffusion coefficients were considered. The conclusions drawn from this study are the following:

1. Divertor

a. In order to obtain a low impurity concentration in the plasma it is necessary to keep the neutral (H_2 molecules) flux coming from the wall as low as possible. Furthermore, for efficient divertor operation it is required that only a small fraction of the neutral generated in the divertor should return to the plasma, i.e. high divertor chamber pumping speed. In addition, for low R_d and R_w, the impurity level can be decreased by enhancing the cross field diffusion coefficient, which may be achieved by destroying the magnetic surfaces with resonant helical windings.[33]

b. The optimum divertor is the one with unload efficiency close to 1 and ionization probability between .5 and 1, i.e. the impurity concentration in the plasma is lower for a divertor with $\eta^u \sim 1$ and $P_z^i \sim .5$ and 1 than for a divertor with $\eta^u \sim .5$ and 1 and $P_z^i = 1$.

c. The major heat loss is by transport to the divertor. Therefore,

the collector plates and the exhaust channels of the divertor should be able to withstand high energy fluxes.

d. The thickness of the "scrape off" region that is required to provide a certain impurity level is determined by both the cross field diffusion coefficient and the particle residence time.

e. As expected, the higher the cross field diffusion, the wider should be the "scrape off" thickness. This study shows that by keeping $\frac{\delta_s}{\sqrt{D}}$ constant the divertor parameters remain unchanged.

f. We find, as expected, that for a given particle and heat flux escaping from the plasma, the ionization probability, P^i, can be improved by increasing the particle residence time. Furthermore, P^i increases as the neutral source coming from the edge (reflected neutral from the wall, backflow from the divertor or gas puffing) increases. Finally, in order to reduce the ionization length in the "scrape off" region, the electron density should be kept as high as possible. This can be achieved by increasing either the particle flux out of the plasma or the "scrape off" thickness.

g. The heavier the impurity, the higher is the ionization probability of the "scrape off" region and the smaller should be the residence time.

h. Injection of small cold neutral source at the wall is found to be beneficial for high z impurity control.

i. The electron temperature drops faster in the "scrape off" region than the ion temperature, this is due to the sheath formation and radiation losses.

j. The plasma ion density attenuates faster for low ion residence time in the scrape off region.

Some of the conclusions concerning the neutral gas blanket are:

a. The contamination of the plasma may be reduced in the presence of a neutral gas blanket by enhancing the cross field diffusion coefficient.

b. The decrease of the neutral reflection coefficient, R_d, from the wall will reduce the impurity level in the plasma.

c. A large fraction of heat will reach the first wall through radiation and charge exchange neutrals.

d. The major heat loss is by charge exchange with cold neutrals.

e. The average electron temperature, T_e, is comparable to the ion temperature for low z impurity, and T_e becomes smaller than T_i for high z impurity where radiation losses increase.

f. For a given external neutral source, a higher heat flux out of the plasma requires wider blanket thickness.

g. The blanket temperature drops as the external neutral source increases.

h. For a given average gas blanket temperature, the neutral source required to cool the boundary region decreases as the gas blanket thickness increases.

k. For a given heat and particle flux escaping from the plasma and a given blanket thickness, there is a maximum neutral source above which no steady state solution exists.

l. The ionization probability of the neutral impurity by the gas blanket is unity.

In conclusion both divertor and gas blanket can decrease the level

of impurity in the plasma provided they are properly designed.

The divertor works efficiently when it operates in the unload mode with an ionization probability for the neutral impurity of the order of 50% or more. High pumping speed in the divertor region is required for efficient divertor operation. The impurity level in the plasma decreases as the wall reflection coefficient decreases.

The gas blanket is a good means for impurity control only for low heat and high particle fluxes out of the plasma. For a fixed Γ_p, as Q_p increases the thickness of the gas blanket should increases to a point where it becomes practically impossible to be included in a fusion reactor. More of a point - the thicknesses required to handle reactor level heat fluxes > 1 m, which is impractical.

Table 1

Divertor parameters as a function of heat flux out of the plasma ($\Gamma_p = 2.2 \times 10^{20}$ $m^{-2}sec^{-1}$, $R_w = .2$, $R_d = 1$, $\delta = 30$ cm, $\tau_{||} = .2 \times 10^{-2}$sec, $D_\perp = D_B$, Carbon)

$Q_p(w/m^2)$	$\frac{Q_w}{Q_p}$	$\frac{\Gamma_{cxw} + \Gamma_{iw}}{\Gamma_p}$	$\frac{n_z(o)}{\Gamma_p}$	η^u	P^i_{dt}	P^i_z	P^q
$.1 \times 10^5$			no steady state solution				
$.32 \times 10^5$	.05	.45	$.59 \times 10^{-3}$	.65	1	1	.77
$.16 \times 10^6$	.14	.91	$.58 \times 10^{-3}$	.32	.995	1	.38
$.32 \times 10^6$	.27	1.1	$.15 \times 10^{-3}$	.10	.72	.93	.11
$.16 \times 10^7$	.16	.94	$.57 \times 10^{-5}$	.13	.29	.73	.05

Table 2

Divertor parameters as a function of heat flux out of the plasma ($\Gamma_p = 2.2 \times 10^{20}$ $m^{-2}sec^{-1}$, $R_d = .2$, $R_w = 1$, $\delta_s = 30$ cm, $\tau_{||} = .61 \times 10^{-3}$sec, $D_\perp = D_B$, Iron)

$Q_p(w/m^2)$	$\frac{Q_w}{Q_p}$	$\frac{\Gamma_{cxw} + \Gamma_{iw}}{\Gamma_p}$	$\frac{n_z(o)}{\Gamma_p}$	η^u	P^i_{dt}	P^i_z	P^q
$.16 \times 10^5$			no steady state solution				
$.32 \times 10^5$	.11	.09	$.82 \times 10^{-3}$	.95	.99	1	.77
$.16 \times 10^6$	.04	.38	$.28 \times 10^{-3}$	.69	.98	1	.70
$.32 \times 10^6$	.03	.28	$.25 \times 10^{-3}$	.78	.96	1	.53
$.16 \times 10^7$	.028	.28	$.18 \times 10^{-3}$	.78	.98	1	.47

Table 3

Divertor parameters as a function of particle flux out of the plasma ($Q_p = .16 \times 10^6$ w/m^2, $R_d = .2$, $R_w = 1$, $\delta_s = 30$ cm, $D = D_B$, carbon wall)

Γ_p ($m^{-2}sec^{-1}$)	$\frac{Q_w}{Q_p}$	$\frac{\Gamma_{cxw} + \Gamma_{iw}}{\Gamma_p}$	$\frac{n_z(o)}{\Gamma_p}$	η^u	P^i_{dt}	P^i_z	P^q
2.2×10^{20}	.14	.91	$.58 \times 10^{-3}$	.32	.995	1	.38
1.1×10^{20}	.15	.87	$.27 \times 10^{-3}$	.39	.85	.96	.15
5.5×10^{19}	.11	.82	$.24 \times 10^{-4}$	.36	.36	.78	.09

Table 4

Divertor parameters as a function of particle flux out of the plasma ($Q_p = .16 \times 10^5$ w/m^2, $R_d = .2$, $R_w = 1$, $\delta = 30$ cm, $D_\perp = D_B$, Iron wall)

Γ_p ($m^{-2}sec^{-1}$)	$\frac{Q_w}{Q_p}$	$\frac{\Gamma_{cxw} + \Gamma_{iw}}{\Gamma_p}$	$\frac{n_z(o)}{\Gamma_p}$	η^u	P^i_{dt}	P^i_z	P^q
2.2×10^{20}	.04	.38	$.28 \times 10^{-3}$	.69	.98	1	.70
1.1×10^{20}	.02	.13	$.18 \times 10^{-3}$	.91	.81	1	.50

Table 5.A

Divertor parameters as a function of cross field diffusion coefficient ($Q_p = .16 \times 10^6$ w/m^2, $\Gamma_p = 2.2 \times 10^{20}$ m^{-2}sec^{-1}, $R_d = .2$, $R_w = 1$, $S_{ex} = 0$, carbon)

D	$\frac{Q_w}{Q_p}$	$\frac{\Gamma_{cxw} + \Gamma_{iw}}{\Gamma_p}$	$\frac{n_z(o)}{\Gamma_p}$	η^u	P^i_{dt}	P^i_z	P^d
D_B	.14	.91	$.58 \times 10^{-3}$	.32	.99	1	.38
$D_B/1.5$	.11	.70	$.58 \times 10^{-3}$	.48	.99	1	.51
$D_B/2$	.08	.56	$.58 \times 10^{-3}$	.41	.99	1	.52

Table 5.B $R_d = R_w = .01$

D_B	$.2 \times 10^{-2}$	.42	$.2 \times 10^{-5}$	.58	.992	.998	.29
$D_B/2$	$.15 \times 10^{-2}$	.20	$.98 \times 10^{-5}$	.81	.999	1	.47
$D_B/3$	$.13 \times 10^{-2}$	.11	$.11 \times 10^{-4}$	.90	.999	1	.65

Table 6

Divertor parameters as a function of δ_s and $D_\perp$ ($Q_p = .16 \times 10^6$ w/m^2, $\Gamma_p = 2.2 \times 10^{20}$ m^{-2}sec^{-1}, $R_d = .2$, $R_w = 1$, $S_{ex} = 0$, carbon)

$\frac{\delta}{\sqrt{D_\perp}}$ = constant	$\frac{Q_w}{Q_p}$	$\frac{\Gamma_{cxw} + \Gamma_{iw}}{\Gamma_p}$	$\frac{n_z(o)}{\Gamma_p}$	η^u	P^i_{dt}	P^i_z	P^d
$\delta = 40$ $D_\perp = 1.8$ D_B	.14	.91	$.42 \times 10^{-3}$	.32	.996	1	.31
$\delta = 30$ $D_\perp = D_B$	.14	.91	$.58 \times 10^{-3}$	.32	.995	1	.38
$\delta = 20$ $D_\perp = \frac{D_B}{2.25}$	.14	.91	$.85 \times 10^{-3}$	.32	.994	1	.65
$\delta = 15$ $D_\perp = \frac{D_B}{4}$	.15	.94	1.1×10^{-3}	.29	.994	1	.51

Table 7

Divertor parameters as a function of ion resident time (Q_w = .16 w/m^2, $\Gamma_p = 2.2 \times 10^{20}$ m^{-2}sec^{-1}, $R_d = R_w = .01$, $S_{ex} = 0$, $D_\perp = D_B$, carbon)

$\tau_{\|}$(sec)	$\frac{Q_w}{Q_p}$	$\frac{\Gamma_{cxw} + \Gamma_{iw}}{\Gamma_p}$	$\frac{n_z(o)}{\Gamma_p}$	η^u	P^i_{dt}	P^i_z	P^d
$.23 \times 10^{-2}$	$.2 \times 10^{-2}$	.42	$.7 \times 10^{-5}$	.58	.99	.99	.29
$.29 \times 10^{-3}$	$.1 \times 10^{-2}$	.15	$.1 \times 10^{-5}$	.86	.70	.93	.39
$.29 \times 10^{-4}$	$.1 \times 10^{-3}$	.02	$.2 \times 10^{-7}$	.98	.14	.68	.41

Table 8

Divertor parameters as a function of $\frac{\delta}{\tau_{\|}}$ = constant ($Q_w = .6 \times 10^6$ w/m^2, $\Gamma_p = 2.2 \times 10^{20}$ m^{-2}sec^{-1}, $R_d = .2$, $R_w = 1$, $S_{ex} = 0.$, $D_\perp = D_B$, carbon)

$\frac{\delta}{\tau_{\|}}$ = constant	$\frac{Q_w}{Q_p}$	$\frac{\Gamma_{cxw} + \Gamma_{iw}}{\Gamma_p}$	$\frac{n_z(o)}{\Gamma_p}$	η^u	P^i_{dt}	P^i_z	P^d
$\delta = 30\ \tau_{\|} = .23 \times 10^{-2}$	.14	.91	$.58 \times 10^{-3}$	.32	.995	1	.38
$\delta = 20\ \tau_{\|} = .15 \times 10^{-2}$	.12	.82	$.39 \times 10^{-3}$	.36	.99	1	.36

Table 9

Divertor parameters as a function of "scrape off" thickness (Q_w = .16 x 10^6 w/m^2, Γ_p = 2.2 x 10^{20} m^{-2}sec^{-1}, R_d = .2, R_w = 1, S_{ex} = 0, $D = D_\perp$, carbon

δ (cm)	$\frac{Q_w}{Q_p}$	$\frac{\Gamma_{cxw} + \Gamma_{iw}}{\Gamma_p}$	$\frac{n_z(o)}{\Gamma_p}$	η^u	P^i_{dt}	P^i_z	P^d
15	.30	1.	.2 x 10^{-4}	.06	.33	.72	.04
20	.31	1.1	.84 x 10^{-4}	.05	.51	.85	.08
25	.20	1.08	.58 x 10^{-3}	.14	.98	.998	.28
30	.14	.91	.58 x 10^{-3}	.32	.995	1	.38

Table 10

Divertor parameters as a function of "scrape off" thickness (Q_w = .16 x 10^6 w/m^2, Γ_p = 2.2 x 10^{20} m^{-2}sec^{-1}, R_d = .2, R_w = 1, S_{ex} = 0, $D_\perp = D_B$, Iron

δ (cm)	$\frac{Q_w}{Q_p}$	$\frac{\Gamma_{cxw} + \Gamma_{iw}}{\Gamma_p}$	$\frac{n_z(o)}{\Gamma_p}$	η^u	P^i_{dt}	P^i_z	P^d
20	.06	.66	.46 x 10^{-3}	.42	.96	1	.11
25	.05	.50	.38 x 10^{-3}	.58	.978	1	.35
30	.04	.38	.28 x 10^{-3}	.69	.98	1	.70

Table 11

Divertor parameters as a function of backflow coefficient ($Q_w = .16 \times 10^6$ w/m^2, $\Gamma_p = 2.2 \times 10^{20}$ m^{-2}sec^{-1}, $R_w = 1$, $S_{ex} = 0$, $D_\perp = D_B$, carbon)

R_d	$\frac{Q_w}{Q_p}$	$\frac{\Gamma_{cxw} + \Gamma_{iw}}{\Gamma_p}$	$\frac{n_z(o)}{\Gamma_p}$	η^u	P^i_{dt}	P^i_z	P^d
1	.16	1.1	1×10^{-3}	.27	.999	1	.54
.8	.155	1.03	$.87 \times 10^{-3}$	.28	.999	1	.30
.6	.144	.95	$.77 \times 10^{-3}$	.32	.998	1	.29
.4	.14	.91	$.64 \times 10^{-3}$	.33	.997	1	.22
.2	.14	.91	$.58 \times 10^{-3}$	.32	.995	1	.38

Table 12

Divertor parameters as a function of external neutral source ($Q_w = .16 \times 10^6$ w/m^2, $\Gamma_p = 2.2 \times 10^{20}$ m^{-2}sec^{-1}, $R_d = .2$, $R_w = 1$, $D_\perp = D_B$, carbon)

S_{ex} ($m^{-2}sec^{-1}$)	$\frac{Q_w}{Q_p}$	$\frac{\Gamma_{ckw} + \Gamma_{iw}}{\Gamma_p}$	$\frac{n_z(o)}{\Gamma_p}$	η^u	P^i_{dt}	P^i_z	P^d
0	.14	.91	$.58 \times 10^{-3}$	.32	.995	1	.38
5×10^{17}	.14	.91	$.57 \times 10^{-3}$	.32	.995	1	.38
5×10^{18}	.14	.91	$.58 \times 10^{-3}$	.32	.996	1	.37
1×10^{19}	.14	.91	$.60 \times 10^{-3}$	.32	.997	1	.36
1×10^{20}	.15	1.0	$.89 \times 10^{-3}$	.29	.999	1	.31

Table 13

Divertor parameters as a function of external neutral source ($Q_w = .16 \times 10^6$ w/m^2, $\Gamma_p = 2.2 \times 10^{20}$ m^{-2}sec^{-1}, $R_d = .2$, $R_w = 1$, $D_\perp = D_B$, Iron)

S_{ex} ($m^{-2}sec^{-1}$)	$\frac{Q_w}{Q_p}$	$\frac{\Gamma_{cxw} + \Gamma_{iw}}{\Gamma_p}$	$\frac{n_z(o)}{\Gamma_p}$	η^u	P^i_{dt}	P^i_z	P^d
0	.04	.38	$.28 \times 10^{-3}$	.69	.98	1	.70
1×10^{17}	.04	.38	$.27 \times 10^{-3}$	.69	.98	1	.74
5×10^{17}	.043	.39	$.28 \times 10^{-3}$	.69	.98	1	.62
1×10^{18}	.05	.50	$.31 \times 10^{-3}$	.58	.984	1	.55

Table 14

Divertor parameters as a function of R_d and R_w ($Q_p = .16 \times 10^6 w/m^2$, $\Gamma_p = 2.2 \times 10^{20}\ m^{-2}sec^{-1}$, $S_{ex} = 0$, $\delta = 30$, $D_\perp = D_B$, carbon)

$R_d = R_w$	$\frac{Q_w}{Q_p}$	$\frac{\Gamma_{cxw} + \Gamma_{iw}}{\Gamma_p}$	$\frac{n_z(o)}{\Gamma_p}$	η^u	P^i_{dt}	P^i_z	P^d
1	.16	1.1	$1. \times 10^{-3}$	.27	.999	1	.54
.9	.15	.99	$.81 \times 10^{-3}$	.32	.998	1	.36
.8	.15	.90	$.70 \times 10^{-3}$	.33	.998	1	.35

Table 15

Divertor parameters as a function of $R_d + R_w$ ($Q_p = .16 \times 10^6 w/m^2$, $\Gamma_p = 2.2 \times 10^{20}\ m^{-2}sec^{-1}$, $S_{ex} = 0$, $\delta = 30$, $R_d = .2$, $D_\perp = D_B$, iron)

R_w	$\frac{Q_w}{Q_p}$	$\frac{\Gamma_{cxw} + \Gamma_{iw}}{\Gamma_p}$	$\frac{n_z(o)}{\Gamma_p}$	η^u	P^i_{dt}	P^i_z	P^d
1	.04	.38	$.28 \times 10^{-3}$	.69	.98	1	.70
.9	.036	.32	$.25 \times 10^{-3}$	.73	.98	1	.57
.8	.036	.32	$.24 \times 10^{-3}$	.74	.98	1	.54

Table 16

Gas blanket parameters as a function of heat flow out of the plasma ($\Gamma_p = .846 \times 10^{21}$ $m^{-2}sec^{-1}$, $R_w = 1$, $\delta_s = 30$ cm, $D_\perp = D_B$, $S_{ex} = 1 \times 10^{20}$ $m^{-2}sec^{-1}$).

Q_p (w/m^2)	$\frac{Q_w}{Q_p}$	$\frac{\Gamma_{cxw} + \Gamma_{iw}}{\Gamma_p}$	$\frac{n_z(o)}{\Gamma_p}$
$.1 \times 10^5$	no steady state solution		
$.2 \times 10^5$	.78	1.43	$.35 \times 10^{-4}$
$.25 \times 10^5$	.81	1.42	$.34 \times 10^{-4}$
$.4 \times 10^5$	.80	1.41	$.29 \times 10^{-4}$

Table 17

Gas blanket parameters as a function of heat flow out of the plasma ($\Gamma_p = .846 \times 10^{21}$ $m^{-2}sec^{-1}$, $R_w = 1$, $\delta_s = 30$cm, $D_\perp = D_B$, $S_{ex} = 1 \times 10^{17}$ $m^{-2}sec^{-1}$).

Q_p (w/m^2)	$\frac{Q_w}{Q_p}$	$\frac{\Gamma_{cxw} + \Gamma_{iw}}{\Gamma_p}$	$\frac{n_z(o)}{\Gamma_p}$
$.53 \times 10^5$	no steady state solution		
$.70 \times 10^5$	.81	1.42	$.68 \times 10^{-4}$
$.85 \times 10^5$	.96	1.42	$.69 \times 10^{-4}$

Table 18

Gas blanket parameters as a function of particle flux out of the plasma ($Q_p = .25 \times 10^5$ w/m^2, $R_w = 1$, $\delta_s = 30$ cm, $D_\perp = D_B$, $S_{ex} = 1 \times 10^{20}$ m^{-2}sec^{-1}, Carbon wall)

Γ_p (#/m^{2}sec)	$\frac{Q_w}{Q_p}$	$\frac{\Gamma_{cxw} + \Gamma_{iw}}{\Gamma_p}$	$\frac{n_z(o)}{\Gamma_p}$
$.63 \times 10^{21}$	.81	1.43	$.38 \times 10^{-4}$
$.846 \times 10^{21}$	.81	1.42	$.34 \times 10^{-4}$

Table 19

Gas blanket parameters as a function of particle flux out of the plasma ($Q_p = .7 \times 10^5$ w/m^2, $R_w = 1$, $\delta_s = 30$cm, $D_\perp = D_B$, $S_{ex} = 1 \times 10^{17}$ m^{-2}sec^{-1}, Iron wall)

Γ_p (#/m^{2}sec)	$\frac{Q_w}{Q_p}$	$\frac{\Gamma_{cxw} + \Gamma_{iw}}{\Gamma_p}$	$\frac{n_z(o)}{\Gamma_p}$
$.63 \times 10^{21}$	.79	1.41	$.77 \times 10^{-4}$
$.846 \times 10^{21}$	.81	1.42	$.68 \times 10^{-4}$

Table 20

Blanket parameters as a function of crossfield diffusion $D_\perp$
($Q_p = .25 \times 10^5$ w/m^2, $\Gamma_p = .846 \times 10^{21} m^{-2}sec^{-1}$, $R_w = 1$, $\delta_s = 30cm$,
$S_{ex} = 1 \times 10^{20} m^{-2}sec^{-1}$, Carbon wall)

$D_\perp$	$\frac{Q_w}{Q_p}$	$\frac{\Gamma_{cxw} + \Gamma_{iw}}{\Gamma_p}$	$\frac{n_z(o)}{\Gamma_p}$
$D_\perp = D_B$	.81	1.42	$.34 \times 10^{-4}$
$D_\perp = \frac{D_B}{1.5}$	.77	1.419	$.4 \times 10^{-4}$
$D_\perp = \frac{D_B}{2}$	.72	1.41	$.48 \times 10^{-4}$

Table 21

Blanket parameters as a function of cross field diffusion, $D_\perp$
($Q_p = .7 \times 10$ w/m^2, $\Gamma_p = .846 \times 10^{21}$ m^{-2}sec^{-1}, $R_w = 1$,
$S_{ex} = 1 \times 10^{17}$ m^{-2}sec^{-1}, $\delta_s = 30$, Iron wall)

$D_\perp$	$\frac{Q_w}{Q_p}$	$\frac{\Gamma_{cxw} + \Gamma_{iw}}{\Gamma_p}$	$\frac{n_z(o)}{\Gamma_p}$
D_B	.81	1.42	$.68 \times 10^{-4}$
$\frac{D_B}{1.5}$	.83	1.418	$.82 \times 10^{-4}$

Table 22

Blanket parameters as a function of the external neutral source for carbon wall ($Q_p = .25 \times 10^5$ w/m^2, $\Gamma_p = .84 \times 10^{21}$ m^{-2}sec^{-1}, $R_w = 1$, $\delta_s = 30$cm)

S_{ex} (m^{-2}sec^{-1})	$\frac{Q_w}{Q_p}$	$\frac{\Gamma_{cxw} + \Gamma_{iw}}{\Gamma_p}$	$\frac{n_z(o)}{\Gamma_p}$
5×10^{19}	.805	1.40	$.32 \times 10^{-4}$
7.5×10^{19}	.806	1.41	$.33 \times 10^{-4}$
1×10^{20}	.806	1.42	$.34 \times 10^{-4}$
2.5×10^{20}	.795	1.49	$.39 \times 10^{-4}$

Table 23

Blanket parameters as a function of the external neutral source for Iron wall ($Q_p = .7 \times 10^5$ w/m^2, $\Gamma_p = .846 \times 10^{21}$ m^{-2}sec^{-1}, $R_w = 1$, $\delta_s = 30$cm)

S_{ex} (m^{-2}sec^{-1})	$\frac{Q_w}{Q_p}$	$\frac{\Gamma_{cxw} + \Gamma_{iw}}{\Gamma_p}$	$\frac{n_z(o)}{\Gamma_p}$
1×10^{19}	.81	1.42	$.68 \times 10^{-4}$
1×10^{20}	.81	1.42	$.68 \times 10^{-4}$
5×10^{20}	.81	1.45	$.71 \times 10^{-4}$
1×10^{21}	.81	1.43	$.69 \times 10^{-4}$
1×10^{22}	.82	1.48	$.75 \times 10^{-4}$

Table 24

Blanket parameters as a function of blanket thickness ($Q_p = .25 \times 10^5$ w/m^2, $\Gamma_p = .846 \times 10^{21}$ m^{-2}sec^{-1}, $R_w = 1$, carbon wall)

δ_s(cm)	$\frac{Q_w}{Q_p}$	$\frac{\Gamma_{cxw} + \Gamma_{iw}}{\Gamma_p}$	$\frac{n_z(o)}{\Gamma_p}$
20	.83	1.44	$.37 \times 10^{-4}$
25	.813	1.43	$.35 \times 10^{-4}$
30	.806	1.42	$.34 \times 10^{-4}$
35	.806	1.41	$.33 \times 10^{-4}$

Table 25

Blanket parameters as a function of blanket thickness ($Q_p = .7 \times 10^5$ w/m^2, $\Gamma_p = .846 \times 10^{21}$ m^{-2}sec^{-1}, $R_w = 1$, Iron wall)

δ_s(cm)	$\frac{Q_w}{Q_p}$	$\frac{\Gamma_{cxw} + \Gamma_{iw}}{\Gamma_p}$	$\frac{n_z(o)}{\Gamma_p}$
20	.79	1.42	$.64 \times 10^{-4}$
25	.80	1.43	$.69 \times 10^{-4}$
35	.81	1.42	$.68 \times 10^{-4}$

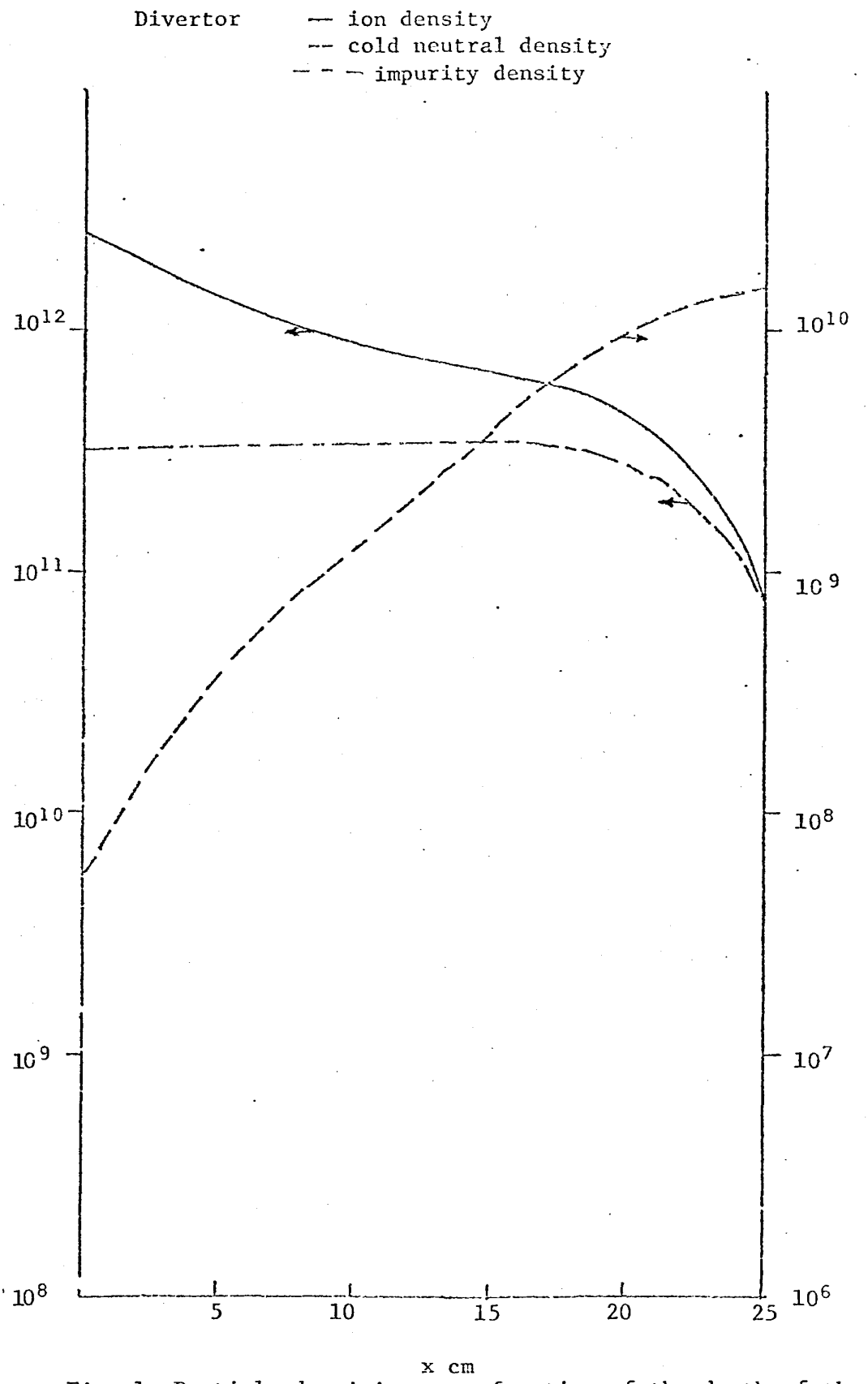

Fig. 1 Particle densities as a function of the depth of the boundary region

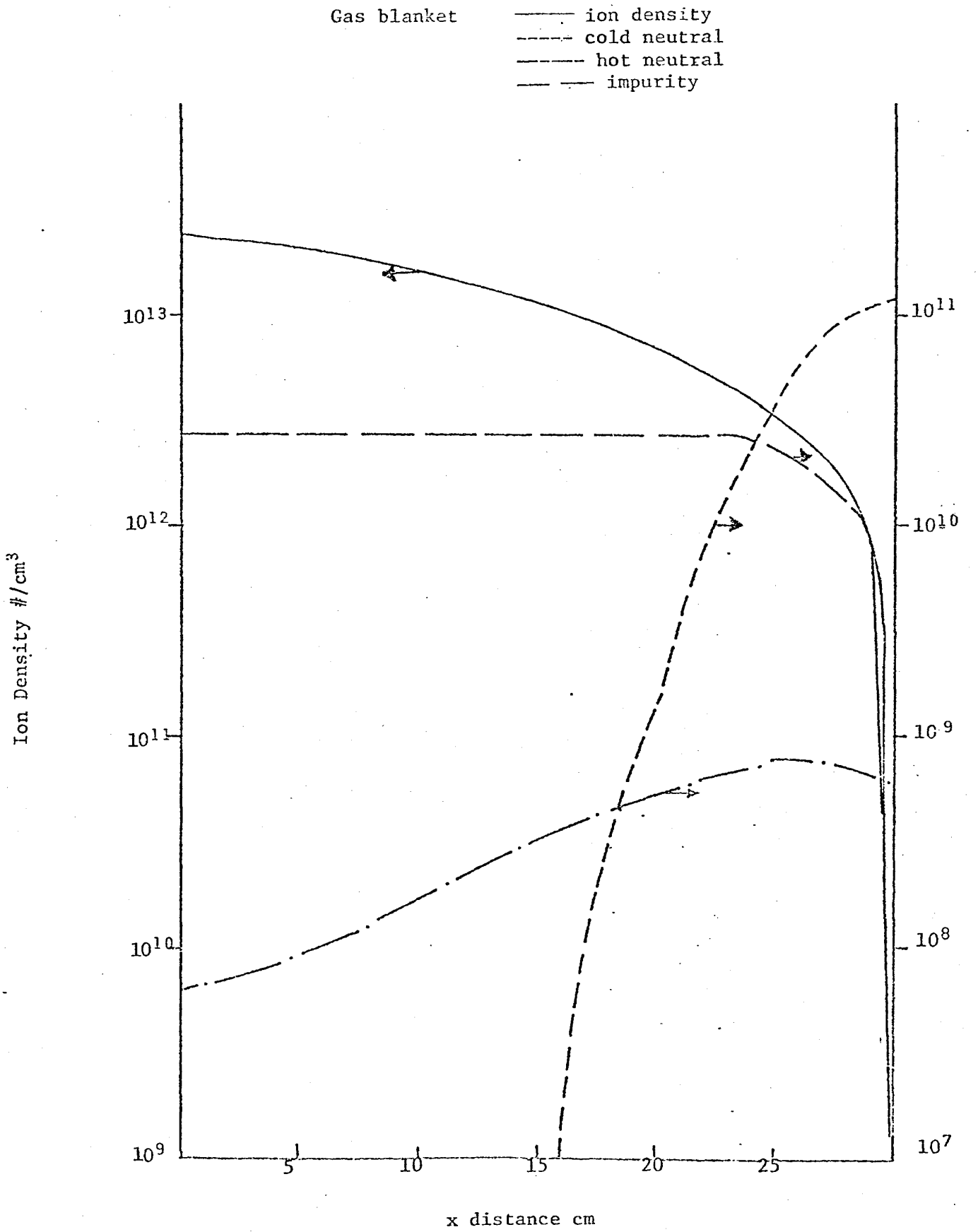

Fig. 2 Particle densities as a function of the depth of the gas blanket.

Fig. 3 Ion density as a function of the depth of the boundary region

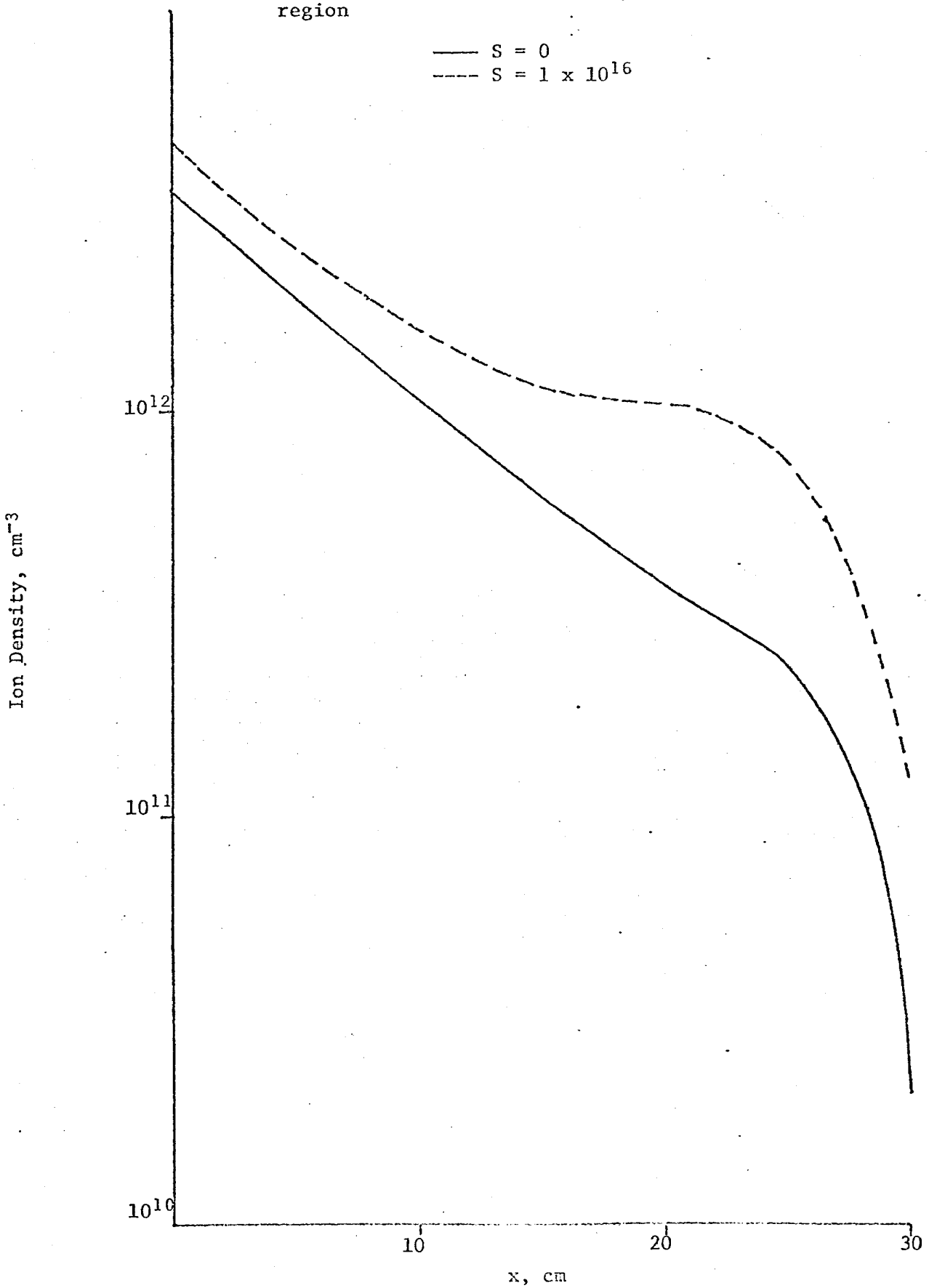

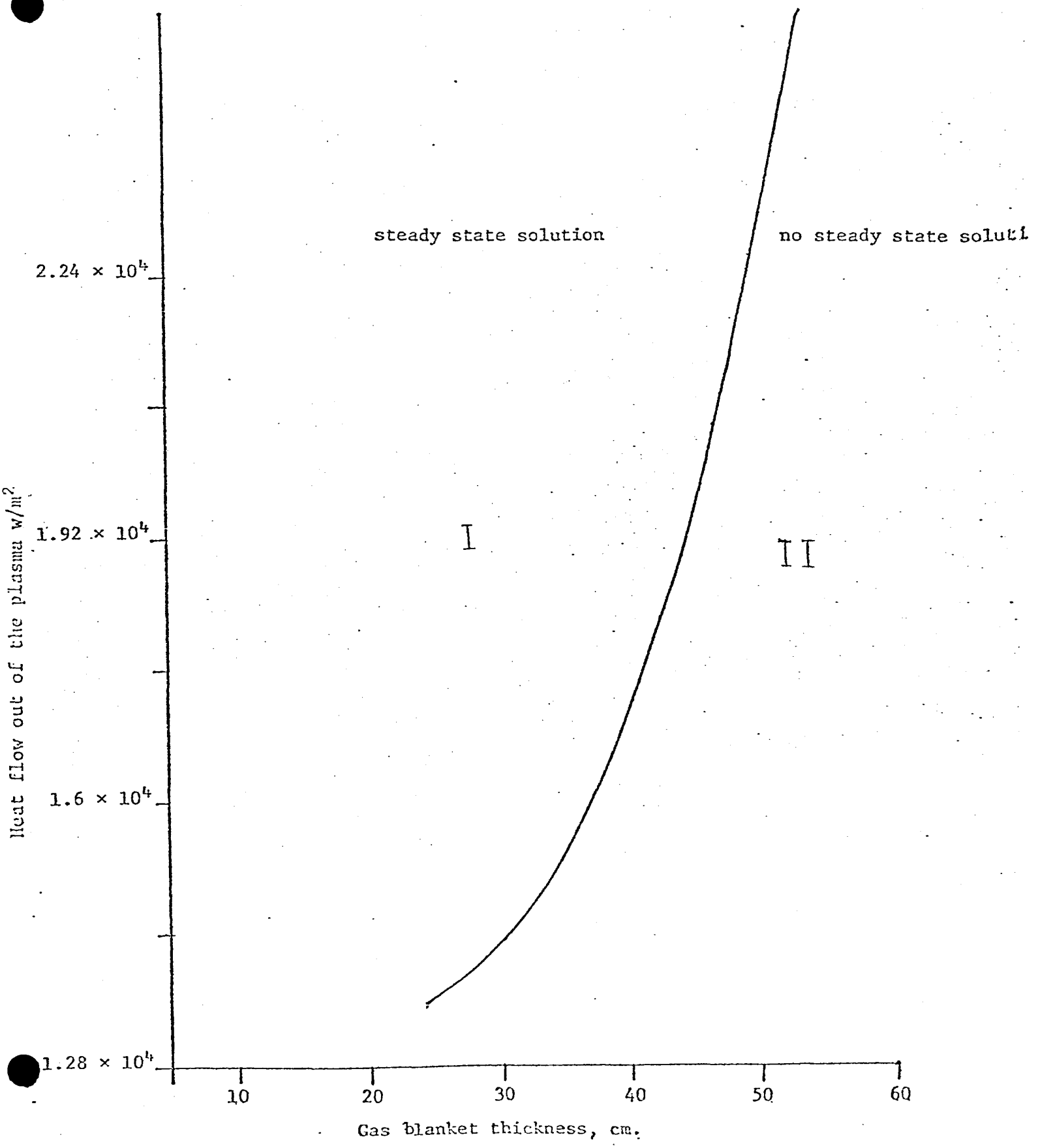

Fig. 4 Minimum Heat Flow out of the Plasma as a Function of the Neutron

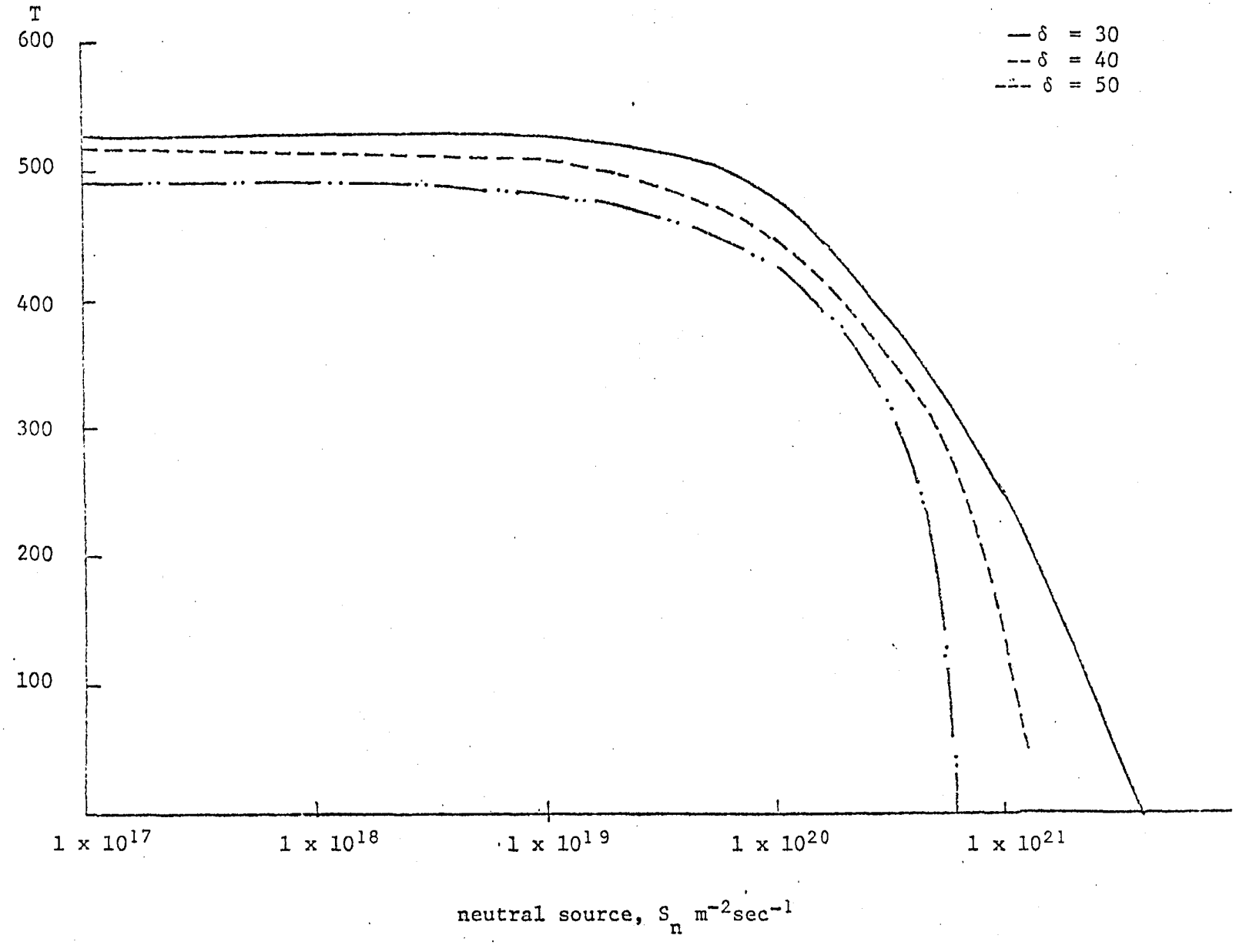

Fig. 5 Average blanket temperature as a function of the external neutral source

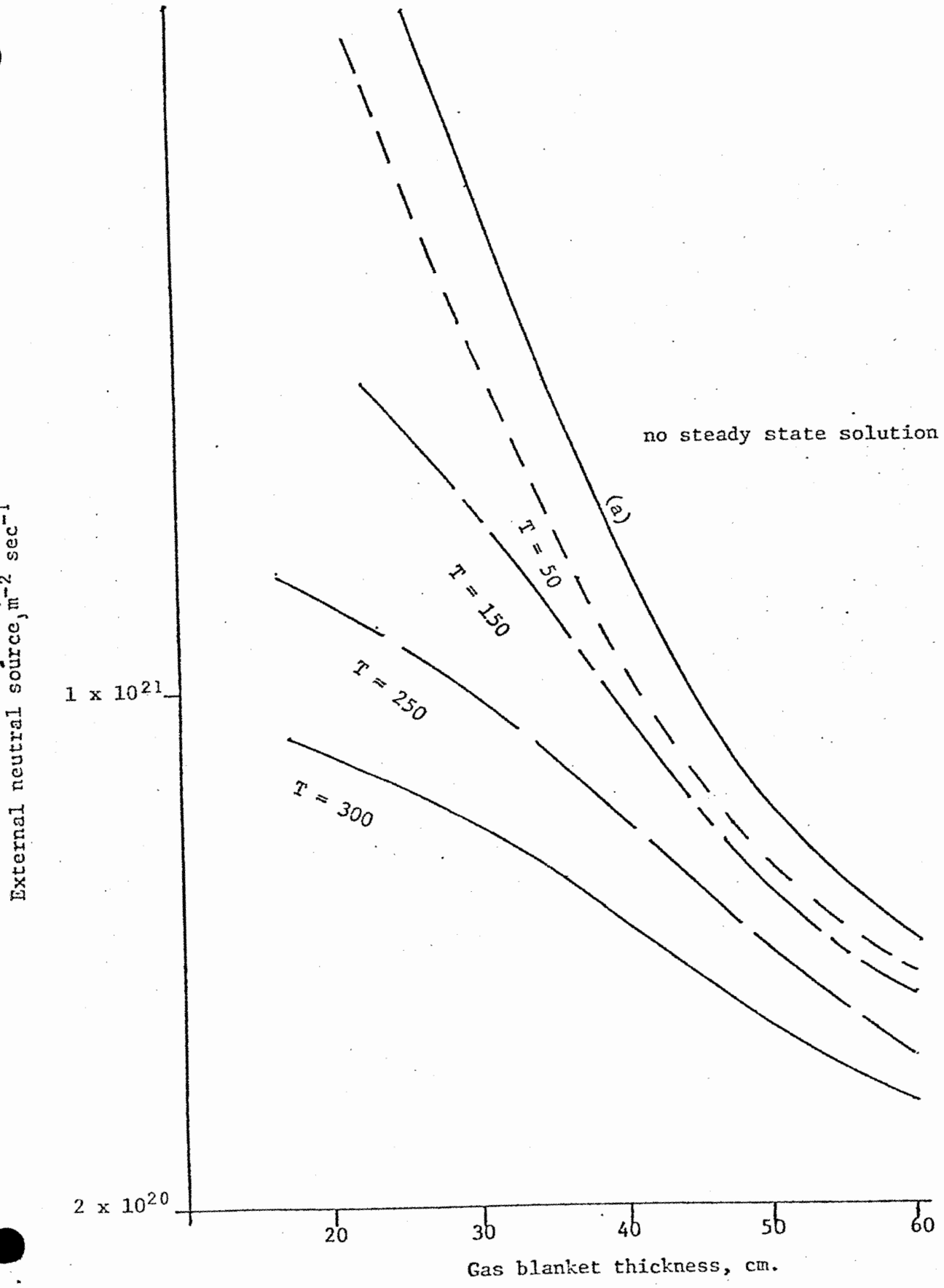

Fig. 6 External Neutral Source as a Function Blanket Thickness.

Fig. 7 Heat flux out of the plasma as a function of the external neutral source.

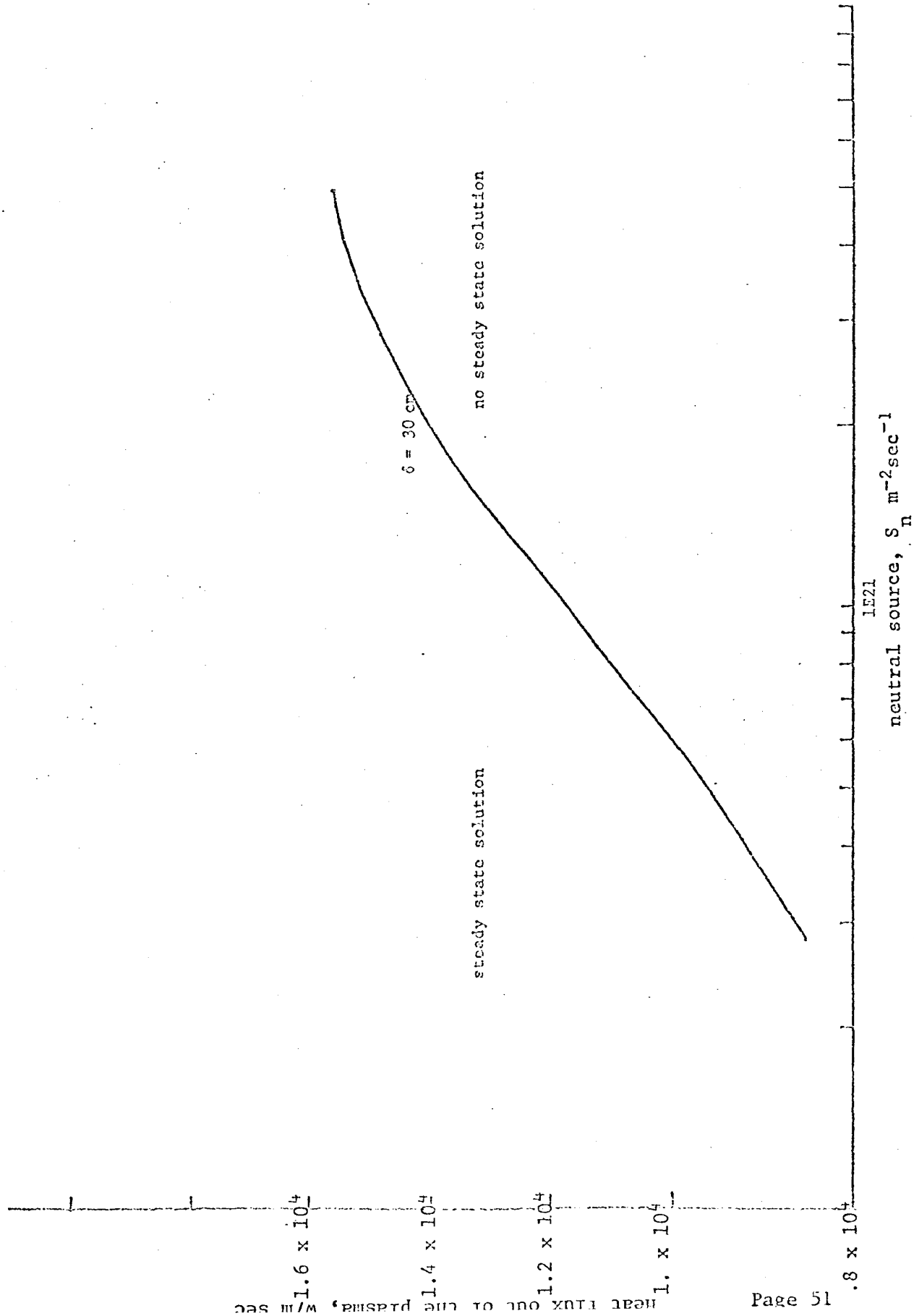

References

1. D. M. Meade, "Effect of High Z Impurities on the Ignition and Lawson Conditions for a Thermonuclear Reactor," Nucl. Fusion, 15, 775 (1975).

2. W. M. Stacey, Jr., et al., "Effect of Plasma Confinement and Impurity Level upon the Performance of a D-T Burning Tokamak Experimental Reactor," Nucl. Fusion, 16, 211 (1976).
W. M. Stacey, Jr., et al., "Impurity Control in Near Term Tokamak Reactor," Proc. ANS Top. Mtg. on Technology of Control Nuclear Fusion, Userda Conf-760935 (1976) p 315.

3. R. V. Jensen, et al., "Critical Impurity Concentration for Power Multiplication in Beam-Heated Toroidal Fusion Reactor," PPPL-1350, Princeton Plasma Physics Laboratory (1977).

4. R. Behrisch, et al., "Plasma Physics and Controlled Nuclear Fusion Research, Vol. II, 229, IAEA, Vienna (1975).

5. D. M. Meade, et al., in Proc. 5th International Conf. Plasma Physics and Controlled Nuclear Fusion Research, IAEA, Vienna (1975) p 605.

6. M. Keilhacker, "Magnetic Divertors," In Proc. School on Tokamak Reactors for Breakeven, Erice (1976).

7. G. A. Emmert, A. T. Mense, J. M. Donhowe, in Technology of Controlled Thermonuclear Fusion (Proc. 1st Topical Meeting,San Diego, 1974), Jr. Nucl. Mater. 53, 39 (1974).

8. C. Cohen, A. Gibson, P. E. Stott, in Controlled Fusion and Plasma Physics (Proc. 5th Europ. Conf., Grenoble, 1972) 1, 6 (1972).

9. PDX, The Poloidal Divertor Experiment, in Large Tokamak Designs,47 (Proc. Joint Euration U.S. Workshop, Gulham, Oxon, U.K. 1974).

10. B. Brandt, C. M. Braams, "The Gas Blanket Concept," Nucl. Fusion, 385 (1974).

11. B. Lehnert, Nucl. Fusion, 8, 173 (1968).

12. T. A. Oliphant, Nucl. Fusion, 13, 521 (1973); Nucl. Fusion, 16, 263 (1973).

13. G. K. Verboom, J. Rem, Nucl. Fusion, 13, 69 (1973).

14. B. Lehnert, Nucl. Fusion, 13, 958 (1973).

15. T. A. Oliphant, J. Nucl. Materials, 53, 62 (1974).

16. F. L. Hinton, et al., Physics of Fluids, 17, 2236 (1974).

17. A. H. Boozer, Physics of Fluids, 19, 1210 (1976).

18. B. Badger, et al., "UWMAK-I, A Wisconsin Toroidal Fusion Reactor Design," University of Wisconsin Report UWFDM-68, Vol. I (1974).

19. A. T. Mense and G. A. Emmert, ORNL/TM-6279 (1978).

20. A. T. Mense, "A Poloidal Divertor Model for Tokamak Fusion Reactors," Ph.D. Thesis, University of Wisconsin 1977).

21. K. Takaymagi and H. Suzuki, "Collection of Cross Section Data for Atomic Processes," IPPY DT-48, Magoya, Japan (1975).

22. C. F. Barnett, et al., "Atomic Data for Controlled Fusion Research," ORNL-5206 and ORNL-5207, Oak Ridge National Laboratory (1977).

23. R. L. Freeman and E. M. Jone, "Atomic Collision Processes in Plasma Physics Experiments," CLM-R137, Gulham Laboratory (1974).

24. H. J. Hanke, "Measurements of Collisional Rate Coefficients in Laboratory Plasmas," Space Science Rev., 13, 565 (1972).

25. W. M. Stacey, Jr., et al., "Impurity Control in Tokamak Reactors," ANL/TM-91 (1977).

26. E. Merzbacker, Quantum Mechanics, 118 (Wiley, 1970).

27. A. Messiah, Quantum Mechanics, 231 (Wiley, 1961).

28. R. E. Langer, "On the Connection Formulas and the Solution of the Wave Equations," Physical Review, 51, 669 (1937).

29. G. I. Bell and S. Glasstone, Nuclear Reactor Theory (Van Nostrand Reinhold, N. Y. 1970).

30. D. Smith, "Physical Sputtering Model for Fusion Reactor Firstwall Material," J. Nucl. Mat., Vol. 76, No. 1, 20-31 (July 1978).

31. D. E. Post, et al., "Steady State Radiative Cooling Rates for Low Density High Temperature Plasmas," PPL-1352, (July 1977).

32. I. P. Shkarofsky, T. W. Johnston, M. P. Bachyinski, "The Particle Kinetics of Plasma," Addison-Wesley, 234 (1966).

33. W. Engelhardt and W. Feneberg, 3rd International Conf. on Plasma Surface Interactions in Controlled Fusion Devices, UKAEA Culham Laboratory, paper 26 (April 1978).